

Geometric Algebra Meets Large Language Models: Instruction-Based Transformations of Separate Meshes in 3D, Interactive and Controllable Scenes

Dimitris Angelis*
ORamaVR, University of Crete, FORTH - ICS
Greece
dimitris.aggelis@oramavr.com

Prodromos Kolyvakis*
ORamaVR
Switzerland
prodromos.kolyvakis@oramavr.com

Manos Kamarianakis
manos.kamarianakis@oramavr.com
ORamaVR, University of Crete, FORTH - ICS
Greece

George Papagiannakis
george.papagianakis@oramavr.com
ORamaVR, University of Crete, FORTH - ICS
Switzerland

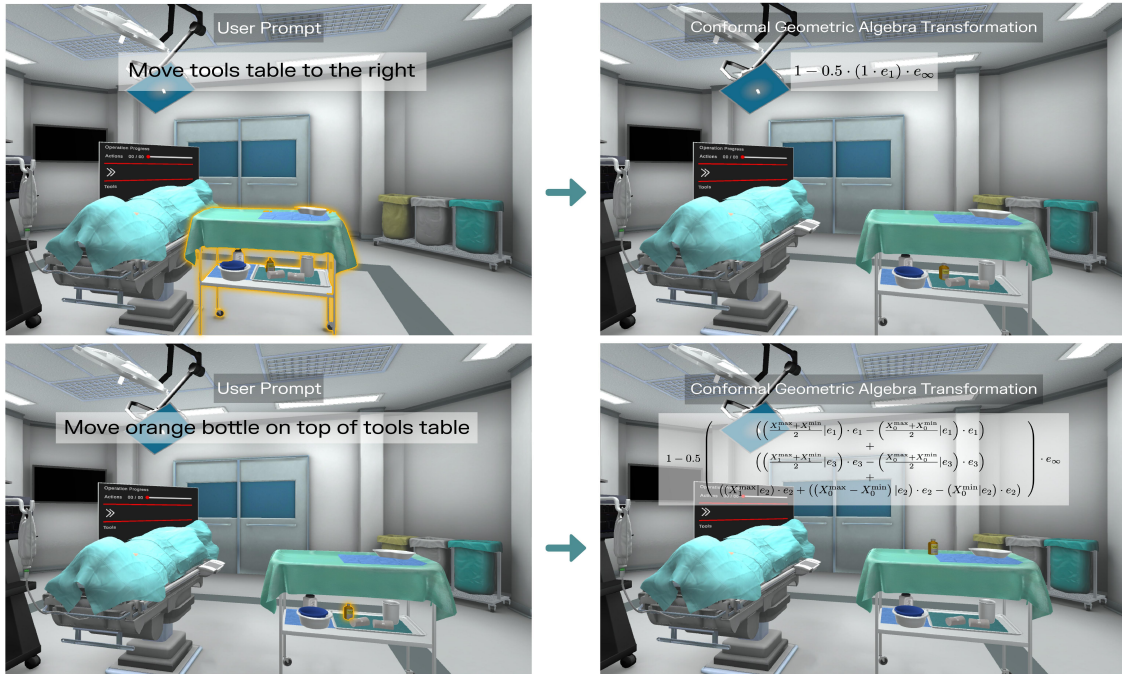


Figure 1: Illustrative demonstration of *shenlong*, our text-based AI assistant for precise object repositioning in scene edits. Displayed are two edit prompts: on top, *moving the tool table to the right*; and on the bottom, *placing the orange bottle on top of the tool table*. The left side of each panel shows the scene before the edit, and the right side shows the scene after the edit. *Shenlong* processes user text queries and generates the corresponding transformations in terms of Conformal Geometric Algebra (CGA), by harnessing a Large Language Model (LLM). The resulting output is then applied to the scene. For each scene, the user’s prompt and the LLM’s CGA-formatted response are presented. Using CGA instead of baseline representations such as transformation matrices, yields better results as shown in Section 5.2.

ABSTRACT

This paper introduces a novel integration of Large Language Models (LLMs) with Conformal Geometric Algebra (CGA) to revolutionize controllable 3D scene editing, particularly for object repositioning tasks, which traditionally requires intricate manual processes and specialized expertise. These conventional methods typically

suffer from reliance on large training datasets or lack a formalized language for precise edits. Utilizing CGA as a robust formal language, our system, *shenlong*, precisely models spatial transformations necessary for accurate object repositioning. Leveraging the zero-shot learning capabilities of pre-trained LLMs, *shenlong* translates natural language instructions into CGA operations which are then applied to the scene, facilitating exact spatial transformations

* Equal Contribution

within 3D scenes without the need for specialized pre-training. Implemented in a realistic simulation environment, shenlong ensures compatibility with existing graphics pipelines. To accurately assess the impact of CGA, we benchmark against robust Euclidean Space baselines, evaluating both latency and accuracy. Comparative performance evaluations indicate that shenlong significantly reduces LLM response times by 16% and boosts success rates by 9.6% on average compared to the traditional methods. Notably, shenlong achieves a 100% perfect success rate in common practical queries, a benchmark where other systems fall short. These advancements underscore shenlong’s potential to democratize 3D scene editing, enhancing accessibility and fostering innovation across sectors such as education, digital entertainment, and virtual reality.

1 INTRODUCTION

Our primary objective is to enable the instruction-based repositioning of objects within 3D, interactive and controllable scenes. Such rearrangement tasks are defined through various descriptors such as object poses, visual representations, descriptive language, or immersive interactions by agents within the desired end states. In this work, we focus primarily on textual instructions. This activity forms a part of the broader challenge in Embodied AI known as the *rearrangement of environments*, where the goal is to configure spaces into predetermined states [Batra et al. 2020]. The ability to reposition objects accurately and intuitively is essential, especially given its significant implications across fields such as digital entertainment, virtual reality (VR), simulation training, and architectural visualization.

Traditionally, this task has demanded intensive manual effort and specialized knowledge, restricting the efficiency and accessibility of 3D scene editing. Recent developments in Foundational Models [Bommasani et al. 2021] represent a paradigm shift, suggesting that complex scene editing could become more intuitive and accessible through simple text-based instructions. However, existing machine learning-based scene representation techniques such as Neural Radiance Fields (NeRFs) [Mildenhall et al. 2020] and Gaussian Splatting [Kerbl et al. 2023] present substantial challenges for precise object repositioning due to their holistic nature, which often obscures individual object details and limits model generalization due to the plurality of possible scenes. [Yu et al. 2020]. In contrast, using separate mesh scene representations provides a viable solution by granting direct access to individual mesh components, which facilitates intuitive interactions and precise alignments tailored to specific editing requirements [Zhai et al. 2024]. However, the overarching question remains: *How effectively can machine learning interact with these separate mesh components for editing?*

The advent of Large Language Models (LLMs) [Jiang et al. 2023; Ramesh et al. 2021; Touvron et al. 2023] offers substantial advancements in human-computer interaction by utilizing linguistic proxies to facilitate instruction-based applications [De La Torre et al. 2024; Durante et al. 2024; Gong et al. 2024; Hong et al. 2023b; Yang et al. 2023]. Moreover, LLMs have significantly contributed to the field of Neurosymbolic AI [Garcez and Lamb 2023; Sheth et al. 2023], enhancing our capability to transform linguistic instructions into precise symbolic representations that bridge the gap between LLMs’

comprehensive understanding abilities and the precision required for complex spatial transformations [Dziri et al. 2023; Hong et al. 2023a; Jignasu et al. 2023]. This LLM - Neurosymbolic AI integration prompts a critical inquiry into the optimal symbolic notation that encapsulates geometric transformations in a manner that LLMs can readily interpret. Geometric Algebra (GA), also known as Clifford Algebra, provides a robust mathematical structure ideal for managing transformations and interactions of geometric objects, which has been widely applied in Computer Graphics [Gunn and De Keninck 2019; Hildenbrand and Rockwood 2022; Papaefthymiou et al. 2016; Papagiannakis 2013].

In this paper, we use a specific GA model called *3D Conformal Geometric Algebra* (CGA) to effectively integrate intuitive linguistic instructions with precise geometric operations, offering a more accessible method for editing separate mesh 3D scenes. This method utilizes the zero-shot learning capabilities of Large Language Models (LLMs), which allows for adaptability to new 3D environments without the requirement for scene-specific training. Our **principal contribution** is the development of shenlong, a system tailored for separate mesh scene editing, particularly designed for object repositioning through textual descriptions. Integrated within the ThreeDWorld (TDW) framework [Gan et al. 2021], shenlong supports the Unity3D Engine and enhances VR-ready 3D scene interaction capabilities. Through rigorously designed experiments, we show that shenlong markedly surpasses existing LLM-based alternatives, including those used in NVIDIA’s Omniverse, in terms of object repositioning within 3D and interactive scenes. A critical aspect of our work is the detailed examination of the limitations currently faced by LLM solutions in object repositioning tasks. Furthermore, we illustrate that LLMs can proficiently generate and manipulate CGA operations with minimal input. Ultimately, our research marks a significant advancement towards democratizing the creation and manipulation of digital environments by simplifying the complex technicalities traditionally involved in 3D scene editing.

2 RELATED WORK

We now present the background pertinent to our research, outlining the foundational concepts and related advances in the field.

2.1 Agent-Driven Object Rearrangement

In the realm of object rearrangement, understanding reusable abstractions through geometric goal specifications ranges from simple coordinate transformations to complex multi-object scenarios [Batra et al. 2020]. Chang et al. [2023] approach rearrangement as an offline goal-conditioned reinforcement learning problem where actions rearrange objects from an initial setup in an input image to conform to a goal image’s criteria. Kapelyukh and Johns [2023] propose learning a cost function through an energy-based model to favor human-like object arrangements. Simeonov et al. [2023] address rearrangement tasks using Neural Descriptor Fields [Simeonov et al. 2022], assigning consistent local coordinate frames to task-relevant object parts, localizing these frames on unseen objects, and aligning them through executed actions. Furthermore, Zhai et al. [2024] integrate scene graphs with diffusion processes for editable generative models, yet require extensive training and access to the complete scene graph, highlighting the efficiency of

our localized transformation approach. Diverging from methods that depend on extensive scene-specific training, our approach leverages the generalization capabilities of LLMs to simplify object repositioning tasks. In contrast to Kwon et al. [2024], who limit their LLM applications to Euclidean spaces for predicting end-effector poses, and Mavrogiannis et al. [2023], who necessitate numerous and cumbersome predefined predicates for translating cooking instructions into Linear Temporal Logic, our method exploits CGA and decomposes repositioning tasks into a minimal set of primitive transformations. Unlike the LLMR approach [De La Torre et al. 2024], which uses specialized LLMs to generate C# Unity code for scene creation and editing, our method avoids direct code generation, thereby ensuring precise scene manipulation without the complexities of writing and debugging code.

2.2 Machine Learning Applications of Geometric Algebra

The incorporation of GA into neural computation was initially introduced in [Pearson and Bisset 1994], with subsequent developments introducing multivector-valued neurons for radial basis function networks [Corrochano et al. 1996], multilayer perceptrons (MLPs) [Buchholz 2000; Buchholz and Sommer 2001], and various neural network architectures [Bayro-Corrochano 2001; Buchholz and Le Bihan 2008; Buchholz and Sommer 2008; Buchholz et al. 2007]. Currently, GA-based neural networks have been applied in various domains, including signal processing [Buchholz and Le Bihan 2008], robotics [Bayro-Corrochano et al. 2018], partial differential equation modeling [Brandstetter et al. 2022], fluid dynamics [Ruhe et al. 2023], and particle physics [Ruhe et al. 2024]. Furthermore, novel GA-based architectures such as multivector-valued convolutional neural networks (CNNs) [Li et al. 2022; Wang et al. 2021], recurrent neural networks [Kuroe 2011; Zhu and Sun 2016], and transformer networks [Brehmer et al. 2024; Liu and Cao 2022] have been introduced, demonstrating the versatility and efficacy of GA in enhancing neural network capabilities for geometrically oriented tasks. Unlike these approaches, our work does not incorporate geometric algebraic components directly within deep learning architectures. Instead, we utilize geometric algebra as a communicative mediator between the LLM and our object rearrangement application. This method emphasizes the use of geometric algebra primarily as a tool to enhance the interaction and translation of complex geometric tasks into understandable formats for the LLM, fostering more effective problem solving capabilities in practical applications. Recently, [Wang et al. 2023] fine-tuned ChatGPT with a large curated collection of textual documents on Geometric Algebra, aimed at developing customized learning plans for students in diverse fields. Our work diverges from the approach of fine-tuning LLMs and instead investigates whether LLMs can effectively utilize geometric algebra for object rearrangement tasks with minimal prompting.

3 CONFORMAL GEOMETRIC ALGEBRA

In his seminal 1872 Erlangen Programme, Felix Klein introduced the revolutionary idea that geometry is best explained by algebra, asserting that algebraic structures govern geometric shapes [Hawkins 1984]. Building on this, quaternions have resurged since the late 20th century due to their compact and efficient representation of

spatial rotations. GA further unifies and extends algebraic systems, including vector algebra, complex numbers, and quaternions, through the concept of *multivectors*. Unlike traditional approaches, which treat scalars, vectors, and higher-dimensional entities separately, GA provides a cohesive framework to uniformly represent and manipulate these entities.

At the heart of GA is the concept of the *geometric product*, which generalizes the dot product and the cross product in Euclidean spaces. Additionally, as all products can be defined using only the geometric one, we need only use the latter one along with addition, scalar multiplication, and conjugation to perform any multivector manipulation. In the context of this work we will be employing CGA, a 32-dimensional extension of quaternions and dual-quaternions [Rooney 2007], where all entities such as vertices, spheres, planes as well as rotations, translations and dilations are uniformly expressed as multivectors [Kamarianakis and Papagiannakis 2021].

For example, assuming the standard CGA basic elements $\{e_1, e_2, e_3, e_4, e_5\}$, a basis of CGA would consist of all 32 (2^5) combinations of up to five of them via geometric product, i.e., $\{1, e_i, e_i e_j, e_i e_j e_k, e_i e_j e_k e_l, e_1 e_2 e_3 e_4 e_5 \text{ for } 1 \leq i < j < k < l \leq 5\}$. For convenience, we define the vectors $e_o = 0.5(e_5 - e_4)$ and $e_\infty = e_4 + e_5$, as well as denote products of basic elements using only subscripts, e.g., $e_{ijk} := e_i e_j e_k$. Using this notation, a sphere s centered at $x = (x_1, x_2, x_3)$ with radius r amounts to the CGA multivector:

$$S = x_1 e_1 + x_2 e_2 + x_3 e_3 + \frac{1}{2}(x_1^2 + x_2^2 + x_3^2 - r^2)e_\infty + e_o. \quad (1)$$

Notice that (a) setting $r = 0$ would yield the respective multivector for the point x and that (b) given S we can extract both x and r .

In this algebra, a translation by (t_1, t_2, t_3) amounts to

$$T = 1 - 0.5(t_1 e_1 + t_2 e_2 + t_3 e_3)e_\infty, \quad (2)$$

thus its inverse would be

$$T^{-1} = 1 + 0.5(t_1 e_1 + t_2 e_2 + t_3 e_3)e_\infty, \quad (3)$$

As noted in Kamarianakis and Papagiannakis [2021], a rotation that would normally be expressed by the unit quaternion:

$$q := a - di + cj - bk. \quad (4)$$

can be represented by the respective *rotor*:

$$R = a + be_{12} + ce_{13} + de_{23}. \quad (5)$$

It then becomes apparent that the inverse of R is

$$R^{-1} = a - be_{12} - ce_{13} - de_{23}. \quad (6)$$

Finally, the multivector:

$$D = 1 + \frac{1-d}{1+d} e_{45} \quad (7)$$

corresponds to a dilation of scale factor $d > 0$ with respect to the origin, whereas it holds that:

$$D^{-1} = \frac{(1+d)^2}{4d} + \frac{d^2-1}{4d} e_{45}. \quad (8)$$

Equations (7) and (8) appear in bibliography with e_{45} replaced by the equivalent quantity $e_\infty \wedge e_o$, where \wedge denotes the *wedge* (or *outer*) product.

To apply transformations M_1, M_2, \dots, M_n (in this order) to an object, we define the multivector $M := M_n M_{n-1} \cdots M_1$, where

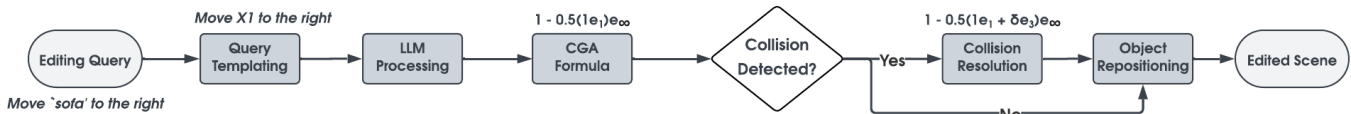


Figure 2: Shenlong’s overview: It generates a CGA transformation after *templating* the query and adds a δ upward translation for a hypothetical Z-axis collision.

all intermediate products are geometric. Shenlong is capable of identifying and generating the intermediate transformations M_i that should be applied to an object and properly returns M . As a composition of rigid body objects and dilations, the resulting multivector is known to be equivalent to a simpler product $M = TRD$ of translation T , a rotation R and a dilation D . By extracting T , R and D , we can express the encapsulated information of M as a translation vector, a unit quaternion and a scale factor which can be ingested by TDW and Unity to visualize the edited object.

To extract T , R and D from a generated CGA product $M = TRD$, we follow the methodology presented in [Kamarianakis et al. 2024]. Specifically, we apply M to a sphere C , centered at origin, with radius equal to 1. The multivector C' corresponding to the transformed sphere can be evaluated via the *sandwich product* $C' = MCM^{-1}$, and we can therefore extract its center x and its radius r . However since C' is the image of the unit, origin-centered, sphere C after applying $M = TRD$, i.e., first a dilation by D , then a rotation by R and finally a translation by T , its radius should be equal to the scaling factor of D and its center should be the translation vector corresponding to T . Since T and D are therefore known, along with $M = TRD$, we can evaluate $R := T^{-1}MD^{-1}$ and therefore the corresponding unit quaternion using (4) and (5).

4 METHODOLOGY

Below we provide the high-level overview of our system, illustrated in Figure 2. When shenlong accepts a query, e.g., *move the ‘sofa’ to the right*, it replaces each object name with a corresponding variable, such as *move X1 to the right*. Shenlong accepts object names enclosed in quotes and sequentially assigns new variables for each unique match found. The templated queries generated allow the LLM to perform symbolic reasoning. Following the substitution of object names with variables, shenlong prompts an LLM to generate the corresponding CGA transformations for the user’s query.

It should be noted that shenlong operates at a local level, lacking a comprehensive understanding of other objects in the scene. While this approach enhances processing efficiency, it may result in collisions with other objects. To address this, we observe that the fuzziness of queries, such as *move the ‘sofa’ to the right*, allows for multiple possible solutions. Upon detecting a collision, shenlong explores perturbed transformations to resolve the issue, e.g., a δ upward translation on Z-axis, ensuring minimal deviation from the intended initial transformation. As a final remark, the proposed system is integrated within the ThreeDWorld (TDW) framework [Gan et al. 2021], supports Unity3D Engine and fosters VR-ready 3D scenes, augmenting human VR interaction.

4.1 LLM Processing & CGA Formulation

Shenlong harnesses CGA to express spatial transformations in a 3D environment, leveraging the precision of this rigorous mathematical framework. Shenlong replaces object names with variables; a vital step for abstracting the user’s intent and preparing the data for algebraic processing. Each object X_i in the scene is represented by an axis-aligned bounding box defined by two points, X_i^{\max} and X_i^{\min} , which encapsulate the object’s spatial extent. This bounding box model simplifies the calculation of movements and rotations by providing clear, definable limits to each object’s position.

Through careful prompting, we instruct the LLM on the key facts and operations of CGA. The complete prompt template is provided in Figure 5. Below are some key remarks. We explained how coordinate extraction can utilize the inner product $|$ operation to precisely isolate spatial coordinates. For example, $(X_1^{\max}|e_2)$ corresponds to the y coordinate of X_1^{\max} . Additionally, we defined the outer (or wedge) product, which establishes planes for rotational operations, and details the mechanisms for both translation and rotation rotors. These rotors are not only defined individually but are also combined through rotor composition, enabling complex sequential transformations essential for accurate scene manipulation. To effectively guide the LLM in utilizing the rotation and translation rotors, we provided a total of five illustrative examples. These include a single example each of rotation and translation to demonstrate basic movements, one compositional example that integrates both types of transformations, and two additional examples addressing more complex, fuzzy queries, such as *move on top of* and *move next to another*. This small diverse set of examples ensures the LLM effectively understands and implements the necessary algebraic operations for object repositioning. Despite the limited number of examples, i.e., only five, we demonstrate in Section 5.2.3 that the LLM can still generalize to complex queries. Finally, the LLM responds by generating a JSON output that includes the specified rotors for composition to be applied to each object.

4.2 Collision Detection Module

Similar to Yang et al. [2023], our system conducts a Depth-First Search (DFS) on a constructed 3D grid surrounding the colliding objects, identifying the first valid solution within the considered search space. We only consider collisions that can be determined using the bounding box information for each object. To prevent placing objects directly on the corners of the 3D grid, we incorporate a fixed buffer zone to ensure adequate spacing during object placement. Each object is described by 6 parameters, corresponding to its axis-aligned bounding box: (x, y, z) for the center coordinates, w , d and h for the width, depth and height. The process starts with initial placements of the target objects and concludes at the first occurrence of a valid placement. We prioritize solutions that are

close to the original configurations, exploring all possibilities and gradually allowing for more distant solutions in a linear progression. Our goal is to minimize disruptions from the initial configuration while preserving the spatial integrity of the scene. This collision resolution operates within a set timeframe (e.g., 0.5 or 1 second). Finally, all transformations are applied.

5 EVALUATION

We conduct comprehensive human evaluations to assess shenlong in object repositioning, engaging 20 annotators: 5 3D designers, 5 game programmers, and 10 individuals outside the gaming and 3D design discipline areas. This study examines shenlong’s proficiency in editing diverse scenes. Through these user studies, we demonstrate that, by harnessing CGA in our prompting strategies, we significantly outperform baseline alternatives, including those made with NVIDIA Omniverse (see Section 5.2.1).

5.1 Experimental Setup

We generated ten diverse scenes using the HOLODECK framework [Yang et al. 2023] for human evaluation, encompassing various settings including living rooms, wine cellars, kitchens, and medical operating rooms. To facilitate the integration of diverse scenes into the TDW framework, we developed a custom importer. For each scene, we created five variations of templated queries, populating them with objects randomly selected from within the scene. We evaluated 50 distinct queries for each scene, resulting in a total of 2,500 scenes (coupled with prompts) for human assessment. For each query, we compared the initial scene with the resulting scene after processing by the two baseline system and shenlong. Examples of the human evaluation are presented in the *Supplementary Material*. For each edited scene, we displayed top-down view images and a 360-degree video view, asking annotators to assess the accuracy of the editing performed. Each object repositioning query was evaluated by five annotators, and a result was considered valid only if all annotators unanimously agreed on the assessment. Due to space limitations, the evaluation queries only are displayed on the y-axis of Figure 4. It should be noted that all preliminary experiments on dilation-related queries with shenlong and other baselines achieved a perfect success rate, leading us to omit these queries. The queries are categorized into five groups, each containing ten queries that evaluate the system’s performance across a progressively increasing difficulty gradient. Below, we provide further details on the group categories used in our analysis:

- **Simple Queries:** Cover basic actions such as rotations and movements along specified axes or planes of a single object.
- **Compositional Queries:** Involve combinations of relative movements and rotations among two or more objects.
- **Fuzzy Queries:** Task systems with interpreting and executing spatial and orientation-specific actions, such as proximity adjustments and directional alignments.
- **Compositional Fuzzy Queries:** Combine multiple elements from compositional and fuzzy queries.
- **Hard Queries:** Represent the most challenging scenarios that test the limits of each system’s processing capabilities.

The classification of “simple” and “composite” queries is based on the study of Manesh et al. [2024] on natural language in virtual

environment creation. Building on this, our work further explores fuzzy and more complex scenarios involving the repositioning of multiple objects.

5.1.1 System Configuration. We employed OpenAI’s GPT-4 model, specifically the *gpt-4-1106-preview* variant, to process scene editing queries. Shenlong executed a distinct API call for each query. The evaluation was done on a laptop with Ubuntu 22.04.4 LTS and AMD Ryzen™ 9 4900HS Mobile Processor (8-core/16-thread, 12MB Cache, 4.3 GHz max boost), NVIDIA® GeForce RTX™ 2060 with Max-Q Design 6GB GDDR6 and 16GB DDR4 RAM at 3200MHz. Rendering was performed using Unity™ 2022.3.9f1.

5.2 Benchmarking

In this section, we assess the performance of our system compared to established baselines. In the following, we provide an overview of the baseline systems against which our solution is measured, the performance metrics that form the criteria for comparison, and a detailed discussion of the results.

5.2.1 Baseline Systems. One of our baseline systems, for comparison is one of the publicly available prompts from NVIDIA’s Omniverse¹. This prompt operates by generating a JSON output that details object placements within a 3D space, similar to our system. Contrary to shenlong, the Omniverse prompt imposes no constraints on the reasoning scheme that the LLM should follow, requesting only the final positions of the objects. The Omniverse prompt accepts input specifications for each object, including its name, dimensions along the X, Y and Z axes, and a centrally located origin point. To ensure this baseline prompt is comparable to our system, we include only points of interest relevant to the scene editing query, rather than the entire scene description as initially done. This refined input approach significantly impacts the LLM’s response time. Our experiments demonstrate that providing only the relevant points of interest leads to a substantial decrease in response time—specifically, an average of 3.3 ± 0.1 times faster—without compromising overall accuracy. Due to these findings, we report results exclusively from this optimized methodology. Finally, we have extended the prompt by incorporating Euler angles for object orientation.

Our second baseline model is derived from recent work showing that LLMs can predict a dense sequence of end-effector poses for manipulation tasks [Kwon et al. 2024]. We extend this concept to object repositioning on 3D scenes, treating it as a form of zero-shot trajectory generation. In this context, we task the LLM with constructing the necessary translation and rotation matrices to define the final trajectory, adapting the underlying techniques to suit scene manipulation objectives. We consider this baseline model to be the closest to our approach, as it guides the LLM to operate using templated functions that correspond to translation and rotation functions within the Euclidean space. This method aligns with our use of structured prompts that direct the LLM to generate specific geometric transformations necessary for scene editing tasks.

¹<https://github.com/NVIDIA-Omniverse/kit-extension-sample-airroomgenerator/blob/main/externals/omni.example.airroomgenerator/omni/example/airroomgenerator/prompts.py>

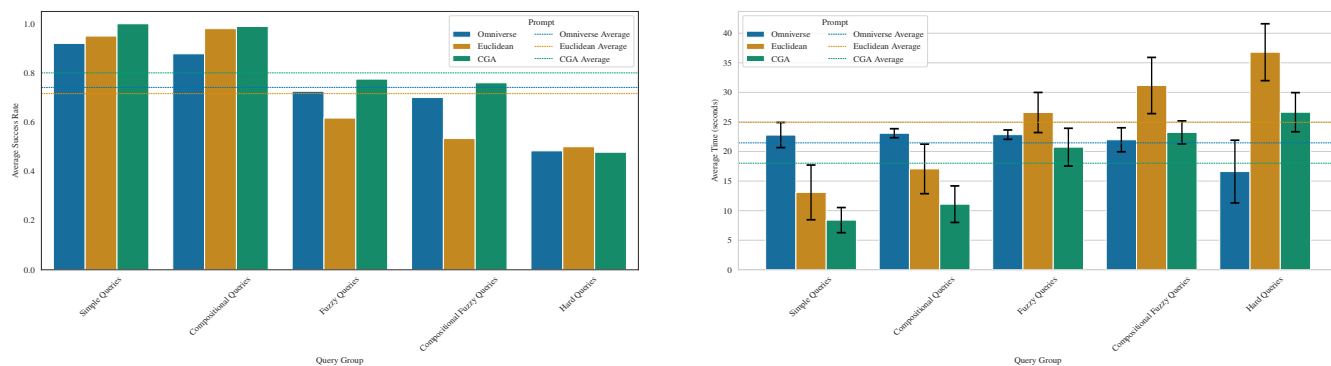


Figure 3: The left chart compares the average success rates, and the right chart compares the average LLM response times for three different systems—Omniverse, Euclidean, and CGA—across five categories of queries: Simple Queries, Compositional Queries, Fuzzy Queries, Compositional Fuzzy Queries, and Hard Queries. Success rates are measured on a scale from 0.0 to 1.0. Horizontal dashed lines indicate the overall mean success rate and response times for each system.

To ensure a fair comparison, we append five specific examples to both the baseline prompts and the final guidelines (refer to Section *Additional Guidance for LLM* in Figure 5). This inclusion is based on findings that demonstrated significant benefits in two distinct cases, enhancing the effectiveness of the LLM in performing scene editing tasks. Due to space limitations, we have included the exact baseline prompts in the *Supplementary Material*.

5.2.2 Performance Metrics. To evaluate the system’s performance, we calculated the success rate per query across the ten different scenes, each with five templated variations. The success rate S for each scene editing query is calculated as follows:

$$S = \frac{1}{M} \sum_{i=1}^M \chi_{\text{correct}}(i)$$

where $\chi_{\text{correct}}(i)$ is the characteristic function that equals 1 if the editing query was performed correctly for the i -th query, and 0 otherwise. Here, M represents the total number of queries, calculated as $M = N \times k$, where N is the number of different scenes considered (10 in our case), and k is the number of variations per scene (5 in our case). Similarly, we compare the average response time across the ten different scenes and their respective variations. The average response time T is calculated by: $T = \frac{1}{M} \sum_{i=1}^M t_i$, where t_i represents the response time for the i -th query. It is commonly noted that LLMs may not always produce valid outputs. We adhere to the standard practice of allowing up to n retries. The reported timings include these retry durations. Notably, in all our experiments, LLMs generated valid prompts within $n = 5$ retries.

5.2.3 Results & Discussion. In this section we present a comprehensive analysis that spans overall performance metrics, detailed evaluations by query group, and granular analyses of individual query performances. These discussions aim to highlight significant findings, interpret the implications of the results, and explore potential areas for further improvement. In all reported figures, we refer to the modified baseline prompts for scene editing as *Omniverse* and *Euclidean*, respectively derived from NVIDIA’s *Omniverse* usage examples and methods akin to zero-shot trajectory generation.

We name the latter *Euclidean* because it closely aligns with our method’s approach in guiding the LLM to generate transformations such as rotations and translations within Euclidean space, in contrast to our use of CGA. Finally, we refer to shenlong’s prompt as *CGA*.

Performance Analysis by Query Group. Figure 3 presents a detailed evaluation of the prompts’ performance across different groups of queries. Each group’s results are analyzed to highlight specific strengths and weaknesses of the system in handling varying complexities. Specifically, the effectiveness and efficiency of the CGA, Omniverse, and Euclidean prompts were evaluated across the five categories of queries: Simple, Compositional, Fuzzy, Compositional Fuzzy, and Hard. We focused on two key performance metrics: average success rate and average response time, providing insights into each system’s scene editing capabilities.

Overall, CGA achieves the highest average success rate of 0.80 and the lowest average response time of 18 seconds ($p < 0.05$), with the results being statistically significant. Interestingly, all prompts exhibited the same overall standard deviation, both in terms of success rate and response time, indicating consistent variability across the different editors. To assess the differences between the systems, we performed Student’s t -tests. In comparison, the Omniverse and Euclidean prompts achieve success rates of 0.74 and 0.72, and average response times of 21.5 seconds and 24.5 seconds, respectively. While the differences in success rates among Omniverse and Euclidean prompts are not statistically significant, the variations in average response times are. We conjecture that the lack of statistical significance in terms of success rates among the systems can be attributed to the nature of the reasoning methods employed. Both the Omniverse and Euclidean prompts rely on classical geometrical reasoning, which may lead to similar levels of performance. In contrast, shenlong utilizes a different approach to reasoning, which not only reflects in its superior performance but also in its statistical significance. This suggests that the distinct reasoning method employed by our system may contribute to its enhanced effectiveness.

Focusing on the success rate metric, CGA consistently exhibits high success rates across all query types, particularly excelling in complex scenarios such as Compositional Fuzzy queries, indicating robust scene understanding. Given that the success rates of the Euclidean and Omniverse systems are not statistically significant, it is evident that CGA provides a relative boost of 9.6% over their average performance. In contrast, Omniverse demonstrates variable performance, experiencing a drop in simpler queries but excelling in fuzzy queries. Conversely, the Euclidean system performs well in simpler queries but shows significant weaknesses in both fuzzy and composite fuzzy queries. CGA appears to integrate the advantages of both systems, performing exceptionally well across simple, fuzzy, and compositional queries. However, it is important to note that with all prompts, ChatGPT-4 shows average performance on hard queries, suggesting potential deficiencies in spatial reasoning.

Regarding response time, Omniverse exhibits consistent average response times across various query groups, regardless of query difficulty, with the notable exception of hard queries, which show the slowest response times. Importantly, CGA demonstrates a 16% relative decrease in response time compared to Omniverse, which is the fastest among the baseline systems. In contrast, the Euclidean prompt demonstrates an increasing trend in response times correlating with query difficulty, peaking with fuzzy, compositional fuzzy, and hard queries. This trend is noteworthy as it suggests that response times increase as query complexity rises. The Euclidean prompt consistently records the longest response times across the complex queries, posing challenges in time-sensitive applications. Meanwhile, the CGA prompt also displays an increasing trend in response times with escalating query difficulty. Notably, it presents slower response times for simple and simple compositional queries despite achieving a 100% success rate. Overall, CGA maintains competitive response times suitable for practical applications, with its response times scaling appropriately with the complexity of queries and achieving the best overall response performance.

Detailed Performance by Individual Query. Figure 4 delves into the performance metrics for each individual query within the groups. This detailed breakdown provides insights into the prompts’ consistency, efficiency, and accuracy in executing scene editing tasks with varying degrees of complexity, facilitating a granular understanding of its operational effectiveness. With regard to the Simple Queries, all systems generally exhibit high success rates for straightforward tasks even in geometrically nuanced rotations such as those over specific planes, e.g., *Rotate X1 over the e1 plane*, with CGA consistently achieving perfect scores. This highlights CGA’s superior handling of precise geometric transformations. The Compositional Queries, which involve a combination of movements and rotations, we see CGA and Euclidean performing robustly, indicating effective integration of complex instructions. Omniverse, however, shows variability, particularly underperforming in scenarios like *Rotate over the e3 plane and move X1 to the right* where it achieves a 0.7 success rate compared to 1.0 by CGA.

In dealing with spatially ambiguous commands, i.e., Fuzzy Queries, Omniverse and CGA outperform Euclidean, especially notable in queries like *Move X1 away from X2* where Euclidean drops to 0 against Omniverse’s perfect score. Interestingly, the Omniverse prompt struggles with the seemingly simple query, *Move X1 on the*

left of X2, displaying a stark contrast to the near-perfect performance of the other systems. Although Omniverse is not presented with a specific *move below* example (only *on top* is provided in their prompts), all systems show generalization capabilities, with CGA achieving the highest success rate of 0.6. Similar generalization is observed with the *Swap X1 and X2* query, where all systems are expected to perform well given their operational logic at the coordinate level; however, Omniverse shows surprisingly lower performance. In contrast, while the Euclidean and CGA systems perform less effectively on the *Move X1 near X2* query, Omniverse excels with perfect success rates. Lastly, all prompts consistently fail the *Rotate X1 to face X2* query. Intriguingly, despite being equipped with Euler angles, Omniverse also fails, suggesting a significant challenge area for current scene editing technologies.

The Compositional Fuzzy Queries category presents a notable challenge, combining fuzzy directives with multiple actions. In this category, Omniverse and CGA show comparable performances, indicating their effective handling of combined directives. However, it is important to note discrepancies in the Euclidean system’s performance. While it achieves good results on individual components of these queries, it performs poorly when actions are combined, as seen in queries like *Move X1 next to X2 and rotate X3 by 90 degrees over the e2 plane* and *Swap X1 and X2 and move X3 on the left by 1 unit*. This inconsistency highlights potential limitations in the Euclidean prompt’s ability to effectively integrate multiple spatial manipulations within a single query.

All systems exhibit challenges with the most demanding Hard Queries, which require intricate arrangements and precise manipulations. Notably, the Euclidean prompt displays extremely inconsistent behavior: it achieves perfect success rates on complex queries such as *Place X1 on top of X2 and X3 below X2* and *Align X1, X2 and X3 in a straight line*, where other systems face difficulties. Conversely, it presents a zero success rate on tasks like *Distribute X1, X2, X3 equally in a circle around X4* or *Arrange X1, X2, X3 in a vertical line, then rotate them by 45 degrees keeping X1 intact*, where other systems manage average performances. This variability suggests that while the Euclidean prompt excels in certain types of spatial reasoning, it may lack robustness in scenarios requiring dynamic spatial transformations or uniform object distribution. These findings underscore the need for further optimization and testing of the Euclidean system to enhance its consistency across a broader range of complex scene editing tasks. In summary, while CGA emerges as the most capable across a broad range of tasks, challenges remain, particularly in Hard and Compositional Fuzzy queries, underscoring the need for further advancements in LLM reasoning capabilities.

6 LIMITATIONS & FUTURE WORK

Object Representations. Currently, our system utilizes multiple intermediate representations of objects, including textual, templated, and bounding box references, requiring exact object names. To enhance this, we plan to implement semantic similarity measures at the token level or more advanced similarity searches using distributed representations. Additionally, we aim to enrich the system with further object information, such as orientation information, to better handle sophisticated queries involving relative rotations.

By improving the system’s grasp of spatial relationships, improved performance in complex scenarios is expected.

System Optimisations. Since we preprocess and create templated queries, it is straightforward to perform query caching optimisations [Mavrogiannis et al. 2023]. We aim to implement query caching optimisations to enhance both the accuracy and responsiveness of our system. We also envision transforming the collision module into a multimodal agent [Yang et al. 2023], enabling nuanced handling of complex scenarios. The agent could be provided with a top-down view of the scene to facilitate finding better resolutions. Lastly, we plan to integrate speech interaction capabilities into our system.

Spatial Reasoning. Our work sheds more light on the spatial reasoning capabilities and limitations of LLMs. Although better and curated prompting could improve performance on more challenging queries, we conjecture that more specialized agents are needed. Future work will explore multimodal alternatives that incorporate top-down views of the scene along with linguistic queries or LLMs fine-tuned on GA [Wang et al. 2023].

REFERENCES

- Dhruv Batra, Angel X. Chang, Sonia Chernova, Andrew J. Davison, Jia Deng, Vladlen Koltun, Sergey Levine, Jitendra Malik, Igor Mordatch, Roozbeh Mottaghi, Manolis Savva, and Hao Su. 2020. Rearrangement: A Challenge for Embodied AI. arXiv:2011.01975 [cs.AI]
- Eduardo Bayro-Corrochano, Luis Lechuga-Gutiérrez, and Marcela Garza-Burgos. 2018. Geometric techniques for robotics and HMI: Interpolation and haptics in conformal geometric algebra and control using quaternion spike neural networks. *Robotics and Autonomous Systems* 104 (2018), 72–84. <https://doi.org/10.1016/j.robot.2018.02.015>
- Eduardo Jose Bayro-Corrochano. 2001. Geometric neural computing. *IEEE Transactions on Neural Networks* 12, 5 (2001), 968–986.
- Rishi Bommasani, Drew A. Hudson, Ehsan Adeli, Russ Altman, Simran Arora, Sydney von Arx, Michael S. Bernstein, Jeannette Bohg, Antoine Bosselut, Emma Brunskill, Erik Brynjolfsson, S. Buch, Dallas Card, Rodrigo Castellon, Niladri S. Chatterji, Annie S. Chen, Kathleen A. Creel, Jared Davis, Dora Demszky, Chris Donahue, Moussa Doumbouya, Esin Durmus, Stefano Ermon, John Etchemendy, Kavin Ethayarajah, Li Fei-Fei, Chelsea Finn, Trevor Gale, Lauren E. Gillespie, Karan Goel, Noah D. Goodman, Shelby Grossman, Neel Guha, Tatsunori Hashimoto, Peter Henderson, John Hewitt, Daniel E. Ho, Jenny Hong, Kyle Hsu, Jing Huang, Thomas F. Icard, Saahil Jain, Dan Jurafsky, Pratyusha Kalluri, Siddharth Karamcheti, Geoff Keeling, Fereshte Khani, O. Khattab, Pang Wei Koh, Mark S. Krass, Ranjay Krishna, Rohith Kudipitudi, Ananya Kumar, Faisal Ladhak, Mina Lee, Tony Lee, Jure Leskovec, Isabelle Levent, Xiang Lisa Li, Xuechen Li, Tengyu Ma, Ali Malik, Christopher D. Manning, Suvir P. Mirchandani, Eric Mitchell, Zanele Muniyikwa, Suraj Nair, Avnika Narayan, Deepak Narayanan, Benjamin Newman, Allen Nie, Juan Carlos Niebles, Hamed Nilforoshan, J. F. Nyarko, Giray Ogut, Laurel Orr, Isabel Papadimitriou, Joon Sung Park, Chris Piech, Eva Portelance, Christopher Potts, Aditi Raghunathan, Robert Reich, Hongyu Ren, Frieda Rong, Yusuf H. Roohani, Camilo Ruiz, Jack Ryan, Christopher R’e, Dorsa Sadigh, Shiori Sagawa, Keshav Santhanam, Andy Shih, Krishna Parasuram Srinivasan, Alex Tamkin, Rohan Taori, Armin W. Thomas, Florian Tramèr, Rose E. Wang, William Wang, Bohan Wu, Jiajun Wu, Yuhuai Wu, Sang Michael Xie, Michihiro Yasunaga, Jiaxuan You, Matei A. Zaharia, Michael Zhang, Tianyi Zhang, Xikun Zhang, Yuhui Zhang, Lucia Zheng, Kaitlyn Zhou, and Percy Liang. 2021. On the Opportunities and Risks of Foundation Models. *ArXiv* (2021). <https://crfm.stanford.edu/assets/report.pdf>
- Johannes Brandstetter, Rianne van den Berg, Max Welling, and Jayesh K Gupta. 2022. Clifford neural layers for pde modeling. *arXiv preprint arXiv:2209.04934* (2022).
- Johann Brehmer, Pim De Haan, Sönke Behrends, and Taco S Cohen. 2024. Geometric Algebra Transformer. *Advances in Neural Information Processing Systems* 36 (2024).
- Sven Buchholz. 2000. Quaternionic spinor MLP. In *Proc. European Symposium on Artificial Neural Networks, 2000*. 377–382.
- Sven Buchholz and Nicolas Le Bihan. 2008. Polarized signal classification by complex and quaternionic multi-layer perceptrons. *International journal of neural systems* 18, 02 (2008), 75–85.
- Sven Buchholz and Gerald Sommer. 2001. Clifford algebra multilayer perceptrons. In *Geometric Computing with Clifford Algebras: Theoretical Foundations and Applications in Computer Vision and Robotics*. Springer, 315–334.
- Sven Buchholz and Gerald Sommer. 2008. On Clifford neurons and Clifford multi-layer perceptrons. *Neural Networks* 21, 7 (2008), 925–935.
- Sven Buchholz, Kanta Tachibana, and Eckhard MS Hitzer. 2007. Optimal learning rates for Clifford neurons. In *Artificial Neural Networks—ICANN 2007: 17th International Conference, Porto, Portugal, September 9–13, 2007, Proceedings, Part I*. Springer, 864–873.
- Michael Chang, Alyssa Li Dayan, Franziska Meier, Thomas L. Griffiths, Sergey Levine, and Amy Zhang. 2023. Hierarchical Abstraction for Combinatorial Generalization in Object Rearrangement. In *The Eleventh International Conference on Learning Representations*. <https://openreview.net/forum?id=FGG6vHp3W9W>
- E Bayro Corrochano, Sven Buchholz, and Gerald Sommer. 1996. Selforganizing Clifford neural network. In *Proceedings of International Conference on Neural Networks (ICNN’96)*, Vol. 1. IEEE, 120–125.
- Fernanda De La Torre, Cathy Mengying Fang, Han Huang, Andrzej Banburski-Fahey, Judith Amores Fernandez, and Jaron Lanier. 2024. LLMR: Real-time Prompting of Interactive Worlds using Large Language Models. In *Proceedings of the 2024 CHI Conference on Human Factors in Computing Systems*. ACM.
- Zane Durante, Bidipta Sarkar, Ran Gong, Rohan Taori, Yusuke Noda, Paul Tang, Ehsan Adeli, Shrinidhi Kowshika Lakshminanth, Kevin Schulman, Arnold Milstein, Demetri Terzopoulos, Ade Famoti, Noboru Kuno, Ashley Llorens, Hoi Vo, Katsu Ikeuchi, Li Fei-Fei, Jianfeng Gao, Naoki Wake, and Qiuyuan Huang. 2024. An Interactive Agent Foundation Model. arXiv:2402.05929 [cs.AI]
- Nouha Dziri, Ximing Lu, Melanie Sclar, Xiang (Lorraine) Li, Liwei Jiang, Bill Yuchen Lin, Sean Welleck, Peter West, Chandra Bhagavatula, Ronan Le Bras, Jena Hwang, Soumya Sanyal, Xiang Ren, Allyson Ettinger, Zaid Harchaoui, and Yejin Choi. 2023. Faith and Fate: Limits of Transformers on Compositionality. In *Advances in Neural Information Processing Systems*, A. Oh, T. Neumann, A. Globerson, K. Saenko, M. Hardt, and S. Levine (Eds.), Vol. 36. Curran Associates, Inc., 70293–70332. https://proceedings.neurips.cc/paper_files/paper/2023/file/deb3c28192f979302c157cb653c15e90-Paper-Conference.pdf
- Chuang Gan, Jeremy Schwartz, Seth Alter, Damian Mrowca, Martin Schrimpf, James Traer, Julian De Freitas, Jonas Kubilius, Abhishek Bhandwadar, Nick Haber, Megumi Sano, Kuno Kim, Elias Wang, Michael Lingelbach, Aidan Curtis, Kevin Tyler Feigels, Daniel Bear, Dan Gutfreund, David Daniel Cox, Antonio Torralba, James J. DiCarlo, Joshua B. Tenenbaum, Josh McDermott, and Daniel LK Yamins. 2021. ThreeDWorld: A Platform for Interactive Multi-Modal Physical Simulation. In *Thirty-fifth Conference on Neural Information Processing Systems Datasets and Benchmarks Track (Round 1)*. <https://openreview.net/forum?id=db1nWAwW2T>
- Artur d’Avila Garcez and Luis C. Lamb. 2023. Neurosymbolic AI: the 3rd wave. *Artificial Intelligence Review* 56, 11 (Nov. 2023), 12387–12406. <https://doi.org/10.1007/s10462-023-10448-w>
- Steven Gong, Qiuyuan Huang, Xiaojian Ma, Hoi Vo, Zane Durante, Yusuke Noda, Zilong Zheng, Song-chun Zhu, Demetri Terzopoulos, Feifei Li, and Jianfeng Gao. 2024. Mindagent: Emergent gaming interaction. In *Proceedings of the North American Chapter of the Association for Computational Linguistics (NAACL) 2024*.
- Charles G. Gunn and Steven De Keninck. 2019. Geometric algebra and computer graphics. In *ACM SIGGRAPH 2019 Courses* (Los Angeles, California) (*SIGGRAPH ’19*). Association for Computing Machinery, New York, NY, USA, Article 12, 140 pages. <https://doi.org/10.1145/3305366.3328099>
- Thomas Hawkins. 1984. The Erlanger Program of Felix Klein: Reflections on its place in the history of mathematics. *Historia Mathematica* 11, 4 (1984), 442–470. [https://doi.org/10.1016/0315-0860\(84\)90028-4](https://doi.org/10.1016/0315-0860(84)90028-4)
- Dietmar Hildenbrand and Alyn Rockwood. 2022. Geometric Algebra Computing for Computer Graphics using GAALOP. In *ACM SIGGRAPH 2022 Courses* (Vancouver, British Columbia, Canada) (*SIGGRAPH ’22*). Association for Computing Machinery, New York, NY, USA, Article 9, 173 pages. <https://doi.org/10.1145/3532720.3535655>
- Sirui Hong, Mingchen Zhuge, Jonathan Chen, Xiauwu Zheng, Yuheng Cheng, Ceyao Zhang, Jinlin Wang, Zili Wang, Steven Ka Shing Yau, Zijuan Lin, Liyang Zhou, Chenyu Ran, Lingfeng Xiao, Chenglin Wu, and Jürgen Schmidhuber. 2023b. MetaGPT: Meta Programming for A Multi-Agent Collaborative Framework. arXiv:2308.00352 [cs.AI]
- Yining Hong, Haoyu Zhen, Peihao Chen, Shuhong Zheng, Yilun Du, Zhenfang Chen, and Chuang Gan. 2023a. 3D-LLM: Injecting the 3D World into Large Language Models. In *Thirty-seventh Conference on Neural Information Processing Systems*. <https://openreview.net/forum?id=YQA28p7qNz>
- Albert Q. Jiang, Alexandre Sablayrolles, Arthur Mensch, Chris Bamford, Devendra Singh Chaplot, Diego de las Casas, Florian Bressand, Gianna Lengyel, Guillaume Lample, Lucile Saulnier, Léo Renard Lavaud, Marie-Anne Lachaux, Pierre Stock, Teven Le Scao, Thibaut Lavril, Thomas Wang, Timothée Lacroix, and William El Sayed. 2023. Mistral 7B. arXiv:2310.06825 [cs.CL]
- Anushrut Jignasu, Kelly Marshall, Baskar Ganapathysubramanian, Aditya Balu, Chinmay Hegde, and Adarsh Krishnamurthy. 2023. Towards Foundational AI Models for Additive Manufacturing: Language Models for G-Code Debugging, Manipulation, and Comprehension. arXiv:2309.02465 [cs.SE]
- Manos Kamarianakis, Nick Lydatakis, and George Papagiannakis. 2024. GA-Unity: A Production-Ready Unity Package for Seamless Integration of Geometric Algebra in Networked Collaborative Applications. arXiv:2406.11560 (June 2024). <https://doi.org/10.48550/arXiv.2406.11560> arXiv:2406.11560 [cs].

- Manos Kamarianakis and George Papagiannakis. 2021. An all-in-one geometric algorithm for cutting, tearing, and drilling deformable models. *Advances in Applied Clifford Algebras* 31, 3 (2021), 58.
- Ivan Kapelyukh and Edward Johns. 2023. SceneScore: Learning a Cost Function for Object Arrangement. In *CoRL 2023 Workshop on Learning Effective Abstractions for Planning (LEAP)*. <https://openreview.net/forum?id=DVKEwUfKQA>
- Bernhard Kerbl, Georgios Kopanas, Thomas Leimkühler, and George Drettakis. 2023. 3D Gaussian Splatting for Real-Time Radiance Field Rendering. *ACM Transactions on Graphics* 42, 4 (July 2023). <https://repo-sam.inria.fr/fungraph/3d-gaussian-splatting/>
- Yasuaki Kuroe. 2011. Models of Clifford recurrent neural networks and their dynamics. In *The 2011 international joint conference on neural networks*. IEEE, 1035–1041.
- Teyun Kwon, Norman Di Palo, and Edward Johns. 2024. Language Models as Zero-Shot Trajectory Generators. In *First Workshop on Vision-Language Models for Navigation and Manipulation at ICRA 2024*. <https://openreview.net/forum?id=5FEHN4e3k>
- Yanping Li, Yue Wang, Rui Wang, Yi Wang, Kaili Wang, Xiangyang Wang, Wenming Cao, and Wei Xiang. 2022. Ga-cnn: Convolutional neural network based on geometric algebra for hyperspectral image classification. *IEEE Transactions on Geoscience and Remote Sensing* 60 (2022), 1–14.
- Qifan Liu and Wenming Cao. 2022. Geometric algebra graph neural network for cross-domain few-shot classification. *Applied Intelligence* 52, 11 (2022), 12422–12435.
- Setareh Aghel Manesh, Tianyi Zhang, Yuki Onishi, Kotaro Hara, Scott Bateman, Jianni Li, and Anthony Tang. 2024. How People Prompt to Create Interactive VR Scenes. *ArXiv abs/2402.10525* (2024). <https://api.semanticscholar.org/CorpusID:267740699>
- Angelos Mavrogiannis, Christoforos Mavrogiannis, and Yiannis Aloimonos. 2023. Cook2LTL: Translating Cooking Recipes to LTL Formulae using Large Language Models. *arXiv preprint arXiv:2310.00163* (2023).
- Ben Mildenhall, Pratul P. Srinivasan, Matthew Tancik, Jonathan T. Barron, Ravi Ramamoorthi, and Ren Ng. 2020. NeRF: Representing scenes as neural radiance fields for view synthesis. In *The European Conference on Computer Vision (ECCV)*.
- Margarita Papaefthymiou, Dietmar Hildenbrand, and George Papagiannakis. 2016. An inclusive Conformal Geometric Algebra GPU animation interpolation and deformation algorithm. *The Visual Computer* 32 (2016), 751–759.
- George Papagiannakis. 2013. Geometric algebra rotors for skinned character animation blending. In *SIGGRAPH Asia 2013 Technical Briefs*. 1–6.
- JK Pearson and DL Bisset. 1994. Neural networks in the Clifford domain. In *Proceedings of 1994 IEEE International Conference on Neural Networks (ICNN'94)*, Vol. 3. IEEE, 1465–1469.
- Aditya Ramesh, Mikhail Pavlov, Gabriel Goh, Scott Gray, Chelsea Voss, Alec Radford, Mark Chen, and Ilya Sutskever. 2021. Zero-Shot Text-to-Image Generation. In *Proceedings of the 38th International Conference on Machine Learning (Proceedings of Machine Learning Research, Vol. 139)*, Marina Meila and Tong Zhang (Eds.). PMLR, 8821–8831. <https://proceedings.mlr.press/v139/ramesh21a.html>
- Joe Rooney. 2007. William Kingdon Clifford (1845–1879). In *Distinguished Figures in Mechanism and Machine Science: Their Contributions and Legacies Part 1*. Springer, 79–116.
- David Ruhe, Johannes Brandstetter, and Patrick Forré. 2024. Clifford group equivariant neural networks. *Advances in Neural Information Processing Systems* 36 (2024).
- David Ruhe, Jayesh K Gupta, Steven De Keninck, Max Welling, and Johannes Brandstetter. 2023. Geometric clifford algebra networks. In *International Conference on Machine Learning*. PMLR, 29306–29337.
- A. Sheth, K. Roy, and M. Gaur. 2023. Neurosymbolic Artificial Intelligence (Why, What, and How). *IEEE Intelligent Systems* 38, 03 (may 2023), 56–62. <https://doi.org/10.1109/MIS.2023.3268724>
- Anthony Simeonov, Yilun Du, Yen-Chen Lin, Alberto Rodriguez Garcia, Leslie Pack Kaelbling, Tomás Lozano-Pérez, and Pulkit Agrawal. 2023. SE(3)-Equivariant Relational Rearrangement with Neural Descriptor Fields. In *Proceedings of The 6th Conference on Robot Learning (Proceedings of Machine Learning Research, Vol. 205)*, Karen Liu, Dana Kulic, and Jeff Ichnowski (Eds.). PMLR, 835–846. <https://proceedings.mlr.press/v205/simeonov23a.html>
- Anthony Simeonov, Yilun Du, Andrea Tagliasacchi, Joshua B. Tenenbaum, Alberto Rodriguez, Pulkit Agrawal, and Vincent Sitzmann. 2022. Neural Descriptor Fields: SE(3)-Equivariant Object Representations for Manipulation. In *2022 International Conference on Robotics and Automation (ICRA)*. 6394–6400. <https://doi.org/10.1109/ICRA46639.2022.9812146>
- Hugo Touvron, Louis Martin, Kevin Stone, Peter Albert, Amjad Almahairi, Yasmine Babaei, Nikolay Bashlykov, Soumya Batra, Prajjwal Bhargava, Shrutit Bhosale, Dan Bikel, Lukas Blecher, Cristian Canton Ferrer, Moya Chen, Guillem Cucurull, David Esiobu, Jude Fernandes, Jeremy Fu, Wenyin Fu, Brian Fuller, Cynthia Gao, Vedanuj Goswami, Naman Goyal, Anthony Hartshorn, Saghar Hosseini, Rui Hou, Hakan Inan, Marcin Kardas, Viktor Kerkez, Madian Khabsa, Isabel Kloumann, Artem Korenev, Punit Singh Koura, Marie-Anne Lachaux, Thibaut Lavril, Jenya Lee, Diana Liskovich, Yinghai Lu, Yuning Mao, Xavier Martinet, Todor Mihaylov, Pushkar Mishra, Igor Molybog, Yixin Nie, Andrew Poulton, Jeremy Reizenstein, Rashi Rungta, Kalyan Saladi, Alan Schelten, Ruan Silva, Eric Michael Smith, Ranjan Subramanian, Xiaoqing Ellen Tan, Binh Tang, Ross Taylor, Adina Williams, Jian Xiang Kuan, Puxin Xu, Zheng Yan, Iliyan Zarov, Yuchen Zhang, Angela Fan, Melanie Kambadur, Sharan Narang, Aurelien Rodriguez, Robert Stojnic, Sergey Edunov, and Thomas Scialom. 2023. Llama 2: Open Foundation and Fine-Tuned Chat Models. *arXiv:2307.09288* [cs.CL]
- Jian Wang, Ziqiang Wang, Han Wang, Wen Luo, Linwang Yuan, Guonian Lü, and Zhaoyuan Yu. 2023. Large Language Model for Geometric Algebra: A Preliminary Attempt. In *Advances in Computer Graphics: 40th Computer Graphics International Conference, CGI 2023, Shanghai, China, August 28 – September 1, 2023, Proceedings, Part IV* (<conf-loc content-type="InPerson">Shanghai, China</conf-loc>). Springer-Verlag, Berlin, Heidelberg, 237–249. https://doi.org/10.1007/978-3-031-50078-7_19
- Rui Wang, Miaomiao Shen, Xiangyang Wang, and Wenming Cao. 2021. Rga-cnns: convolutional neural networks based on reduced geometric algebra. *Sci. China Inf. Sci* 64, 129101 (2021), 1–129101.
- Yue Wang, Fan-Yun Sun, Luca Weihs, Eli VanderBilt, Alvaro Herrasti, Winson Han, Jiajun Wu, Nick Haber, Ranjay Krishna, Lingjie Liu, Chris Callison-Burch, Mark Yatskar, Aniruddha Kembhavi, and Christopher Clark. 2023. Holodeck: Language Guided Generation of 3D Embodied AI Environments. *arXiv preprint arXiv:2312.09067* (2023).
- Alex Yu, Vickie Ye, Matthew Tancik, and Angjoo Kanazawa. 2020. pixelNeRF: Neural Radiance Fields from One or Few Images. <https://arxiv.org/abs/2012.02190> (2020).
- Guangyao Zhai, Evin Pinar Örnek, Dave Zhenyu Chen, Ruotong Liao, Yan Di, Nassir Navab, Federico Tombari, and Benjamin Busam. 2024. EchoScene: Indoor Scene Generation via Information Echo over Scene Graph Diffusion. *arXiv preprint arXiv:2404.00000* (2024).
- Jingwen Zhu and Jitao Sun. 2016. Global exponential stability of Clifford-valued recurrent neural networks. *Neurocomputing* 173 (2016), 685–689.

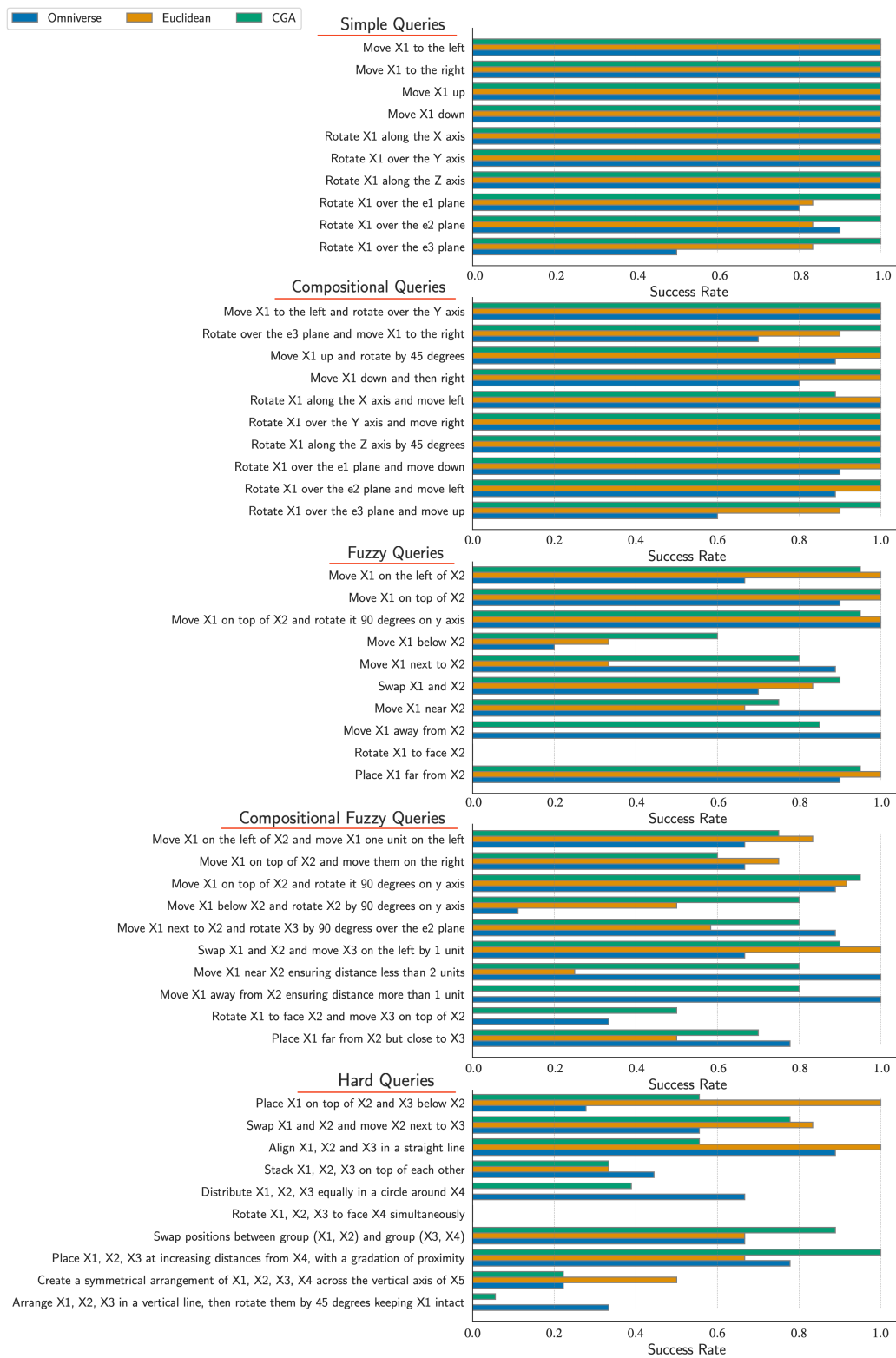


Figure 4: Query resolution performance for different prompts—Omniverse, Euclidean, and CGA—across five query categories: Simple, Compositional, Fuzzy, Compositional Fuzzy, and Hard. Success rate is assessed for each templated query over ten different scenes, with five query variations per scene.

```

### Objective:
You MUST calculate the appropriate transformation for objects in a 3D space using templated variables (`X1`, `X2`, etc.)

You MUST only use a valid combination of the defined algebraic operations.
### Coordinate System:
- **X-axis (`e1`)**: Translates the object LEFT (-) or RIGHT (+).
- **Y-axis (`e2`)**: Translates the object BOTTOM (-) or TOP (+) height wise.
- **Z-axis (`e3`)**: Translates the object BACK (-) or FORWARD (+).
### Defined Algebraic Operations:
1. **Rotation** The rotation rotor  $R(\theta, u, v)$  rotates a vector by an angle  $\theta$  in the plane defined by  $u \wedge v$ .
2. **Translation** The translation rotor  $T(x * e1 + y * e2 + z * e3)$  translates an object along the vector  $x * e1 + y * e2 + z * e3$ .
3. **Coordinate Extraction** Use the inner product  $(x1 | e3) * e3$  to extract the coordinate along the Y-axis.
4. **Outer Product** For independent vectors,  $u \wedge v$  is non-zero and represents an oriented plane.
5. **Commutation** Translation operators commute,  $T(v) * T(w) = T(w) * T(v)$ .
6. **Rotor Composition** Rotors can be combined by multiplication, representing sequential rotations.
### Task Instructions:
1. APPLY the specified T for translation and R for rotation operations, adhering to the defined algebraic operations.
2. DO NOT introduce any variables or constants not explicitly mentioned in the input.
3. USE ONLY the variables names and e1, e2, e3 on the operations.
4. OUTPUT the transformations in JSON format, using key-value pairs for each object and its transformation.
5. USE ONLY the max and min points of an object's bounding box (e.g., X1.max and X1.min) for all calculations.
6. For coordinate extraction, employ the inner product operator |. For instance, use  $(X1.max | e2) * e2$  to extract the Y axis coordinate.
7. CONSIDER the current position of objects when moving one in relation to another. Calculate transformations using the initial locations derived from their bounding box points.
### Example Inputs, Results in JSON format
1. **Input**: 'Translate X1 by 1 unit to the left.'
**Output**: {'X1': 'T(-1 * e1)'}
**Explanation**: The bounding box of X1 is defined by the points X1.max and X1.min. To translate X1 by 1 unit to the left, we must subtract 1 from the X-axis coordinate of both points. Therefore, the transformation is  $T(-1 * e1)$ .
2. **Input**: 'Rotate X1 by 90 degrees around the z-axis.'
**Output**: {'X1': 'R(np.pi/2, e1, e2)'}
**Explanation**: The rotation rotor  $R(\theta, u, v)$  rotates a vector by an angle  $\theta$  in the plane defined by  $u \wedge v$ . In this case, the rotation is 90 degrees in the z-axis is defined as the rotation around e1, e2 plane. Therefore, the transformation is  $R(np.pi/2, e1, e2)$ .
3. **Input**: 'Translate X2 by 1 unit to the right and rotate it by 90 degrees around the z-axis.'
**Output**: {'X2': 'T(1 * e1) * R(np.pi/2, e1, e2)'}
**Explanation**: The bounding box of X2 is defined by the points X2.max and X2.min. To translate X2 by 1 unit to the right, we must add 1 to the X-axis coordinate of both points. Therefore, the translation is  $T(1 * e1)$ . The rotation rotor  $R(\theta, u, v)$  rotates a vector by an angle  $\theta$  in the plane defined by  $u \wedge v$ . In this case, the rotation is 90 degrees in the z-axis is defined as the rotation around e1, e2 plane. Therefore, the rotation is  $R(np.pi/2, e1, e2)$ . Since the rotation must be applied after the translation, the transformation is  $T(1 * e1) * R(np.pi/2, e1, e2)$ .
4. **Input**: 'Move X1 on top of X0.'
**Output**: {'X1': 'T((X0.max+X0.min)/2 - (X1.max+X1.min)/2 + ((X0.max - X0.min) | e2) * e2)'}
**Explanation**: The bounding box of X1 is defined by the points X1.max and X1.min. The bounding box of X0 is defined by the points X0.max and X0.min. To move X1 on top of X0, we must translate X1 by the difference between the center of X0 and X1 and the Y-axis coordinate of X0. Therefore, the transformation is  $T((X0.max+X0.min)/2 - (X1.max + X1.min)/2 + ((X0.max - X0.min) | e2) * e2)$ .
5. **Input**: 'Move X1 next to X0.'
**Output**: {'X1': 'T((X0.max+X0.min)/2 - (X1.max+X1.min)/2 + (X0.max + (X0.max - X0.min) | e1) * e1)'}
**Explanation**: The bounding box of X1 is defined by the points X1.max and X1.min. The bounding box of X0 is defined by the points X0.max and X0.min. To move X1 next to X0, we must translate X1 by the difference between the center of X0 and X1 and the X-axis coordinate of X0 and then add an offset along the e1 plane in order for the objects to not collide with each other. Therefore, the transformation is  $T((X0.max+X0.min)/2 - (X1.max+X1.min)/2 + ((X0.max - X0.min) | e1) * e1)$ .
### Output Format:
The output MUST be formatted as a SINGLE JSON object containing all transformations for each object.
### Additional Guidance for LLM:
- ADHERE strictly to the defined algebraic operations.
- DOCUMENT Each Step: For every action you perform, you MUST provide a clear and numbered list of operations used during your reasoning.
- REVISE any transformation that does not comply with these principles.
- It's **IMPORTANT** to take into consideration all axis when performing relative transformations. Focus on the X **AND** Z axis when moving objects around the room. Make changes in the Y axis when a vertical movement is required. So, for example, when moving an object next to another, you should move it in both the X and Z axis, and when moving an object on top of another, you should move it in the X and Z axis, and also in the Y axis.
- When no axis is defined for rotations, the default axis is the Y-axis which means a rotation in the e1, e3 planes.
- When you want to move or rotate an object along an axis you must use the inner product operator |. For example, to move an object along the Y-axis you must use  $(X1.max | e2) * e2$ .
- When no unit is specified for the translation, the default unit is 1 and for the rotation, the default unit is 90 degrees.

```

Figure 5: Template for Conformal Geometric Algebra Prompts Used by shenlong.

A QUALITATIVE RESULTS

Table 1 and 2 present qualitative results that enhance understanding of the user experience quality, illuminate the evaluation scheme, and clarify the advantages and disadvantages of different prompts. As detailed in Section 4.1 of the paper, each object repositioning query is evaluated by five annotators. A result is considered valid only if there is unanimous agreement among all annotators on the assessment. The first column of Table 1 displays the performance of different prompts—CGA, Euclidean, and Omniverse—respectively, for the query *move 'chair 1' away from the table*. Our annotators unanimously agreed that the Omniverse prompt accurately aligns with the requested query. The CGA prompt correctly interprets the query but leaves the chair relatively close to the table, which is not considered a correct result. In contrast, the Euclidean prompt does not result in any transformation. In the second column, for the second prompt, i.e., *Rotate X1 over the e3 plane and move up*, both CGA and Euclidean adeptly rotate and elevate a book on the top right side of the bookcase, while Omniverse incorrectly rotates it along the wrong axis. Finally, in the third column of Table 1, both CGA and Omniverse successfully relocate the patient table, while Euclidean fails to do so. It can be observed that the Euclidean prompt either fails to alter object relations significantly or misinterprets the queries, even simple ones.

In the first query of Table 2, both CGA and Euclidean accurately position the orange bottle and the vase. In contrast, Omniverse misinterprets the z-axis as the y-axis, resulting in the vase being placed behind the table. In the second column of Table 2, when examining a wine cellar scene, only CGA accurately repositions a mask frame below a city frame. Conversely, the Euclidean approach incorrectly places it adjacent to the other frame, while Omniverse incorrectly identifies the correct axis for movement. Last but not least, we see that for the last query on Table 2, i.e., *move 'barrel 1' far from 'barrel 2' but close to 'barrel 3'*, both Euclidean and Omniverse do not provide appropriate solutions. Importantly, CGA provides a valid solution.

B IMPLEMENTATION DETAILS

The scene editing agent processes user queries like *move sofa to the right*, converting them into a templated format such as "move X1 to the right." This involves matching specific phrases in the query and assigning variables accordingly. We then make an API call to OpenAI's *gpt-4-1106-preview* model via LangChain². The model's JSON response maps edited object variables (e.g., 'X1') to CGA transformations (e.g., 'X1': 'T(-1 * e1)'), where 'T' stands for translation and 'R' for rotation. Next, we transform this symbolic output into executable Python code using the Clifford³ library, replacing variables like 'X' with actual object names and converting 'T' and 'R' into their respective functions. For example, the response might be transformed to `'sofa': 'generate_translation_rotor(-1 * e1)'`. These equations are then applied to the corresponding objects in the scene, implementing the specified transformations. Our system is integrated within the ThreeDWorld⁴ (TDW) framework, using

Unity for rendering, and has been tested in VR with the Oculus Quest 2 HMD to verify scene fidelity and compatibility.

C EUCLIDEAN & OMNIVERSE PROMPTS

As discussed in Section 4.2.1 of the main paper, Figure 6 displays the Euclidean prompt. Additionally, Figures 7 and 8 showcase the prompts from NVIDIA's Omniverse⁵. For a fair comparison, both sets of prompts are presented with the main guidelines and examples, similar to the CGA prompt shown in Figure 5 of the main paper.

²<https://github.com/langchain-ai/langchain>

³<https://github.com/pygae/clifford>

⁴<https://github.com/threedworld-mit/tdw>

⁵<https://github.com/NVIDIA-Omniverse/kit-extension-sample-airoomgenerator/blob/main/exts/omni.example.airoomgenerator/omni/example/airoomgenerator/prompts.py>









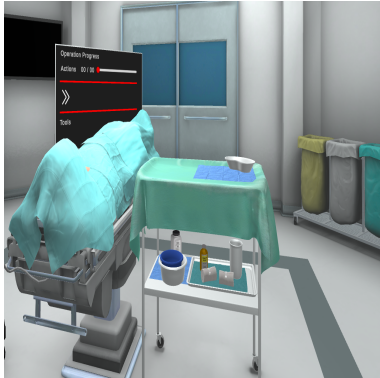



Query	Move 'chair 1' away from table	Rotate 'book 1' over e3 plane and move up	Move 'tools table' away from 'patient' ensuring a distance of at least 1 unit
Initial Scene			
CGA			
Euclidean			
Omniverse			

Table 1: Results across three different scenes for each prompt and for each system.




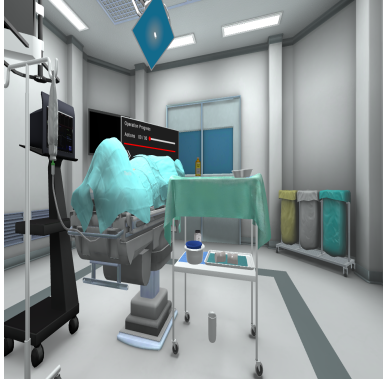


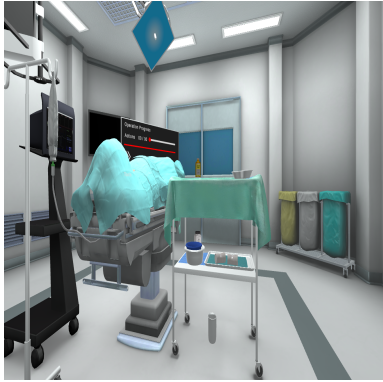





Query	Place 'orange bottle' on top of 'tools table' and 'vase' below 'tools table'	Move 'mask frame' below 'city frame'	Move 'barrel 1' far from 'barrel 2' but close to 'barrel 3'
Initial Scene			
CGA			
Euclidean			
Omniverse			

Table 2: Results across three different scenes for each prompt and for each system.

You are a sentient AI capable of manipulating the placement of objects within a scene through matrix calculations. These calculations produce transformation matrices in Euclidean 3D space that conform to user commands.

AVAILABLE FUNCTIONS:
You **MUST** remember that this conversation is a monologue, with you in control. I am unable to assist with any questions. You **MUST** independently produce the final output using available information, common sense, and general knowledge. You **MUST** use the following details for each object to generate the output:

- **TRS_matrix****: A 4x4 transformation matrix that represents the translation, rotation, and scaling of an object in 3D space.
- **Box****: A list of two vectors, where the first vector represents the minimum point of the bounding box and the second vector the maximum point. Use ``X1.Box[0]`` to access the minimum point and ``X1.Box[1]`` for the maximum point. For coordinates, ``X1.Box[0][0]`` accesses the x-coordinate of the minimum point, etc.

General Functions:

- **translation_matrix(x, y, z)****: Generates a translation matrix for the specified x, y, and z values.
- **rotation_matrix(x, y, z)****: Produces a rotation matrix for the given x, y, and z values.
- **scaling_matrix(x, y, z)****: Creates a scaling matrix for the specified x, y, and z values.

ENVIRONMENT SET-UP:
The 3D coordinate system is defined as follows:

- The x-axis extends horizontally to the right.
- The y-axis extends vertically towards the ceiling.
- The z-axis also extends vertically, but upwards.

COLLISION AVOIDANCE:
For tasks involving multiple objects, you **MUST** ensure no collisions by considering each object's bounding box.

INITIAL PLANNING:
You **MUST** detail the initial planning and reasoning for the task before generating calculations.

OUTPUT FORMAT:
YOU **MUST** provide a sequence of calculations for generating the transformation matrix for each object in the scene in JSON format.

EXAMPLES:

- **Input****: "Translate X1 2 units to the right."
****Output****:
``{'X1': ' X1.TRS_matrix @ translation_matrix(2, 0, 0)}``
****Explanation****: The translation matrix is applied to the object X1 to move it 2 units to the right.
- **Input****: "Rotate X1 90 degrees around the z-axis."
****Output****:
``{'X1': 'X1.TRS_matrix @ rotation_matrix(0, 0, 90)}``
****Explanation****: The rotation matrix is applied to the object X1 to rotate it by 90 degrees around the z-axis.
- **Input****: "Translate X2 1 unit to the right and rotate it by 90 degrees around the z-axis."
****Output****:
``{'X2': ' X2.TRS_matrix @ translation_matrix(1, 0, 0) @ rotation_matrix(0, 0, 90)}``
****Explanation****: The translation matrix is applied to the object X2 to move it 1 unit to the right, followed by a rotation of 90 degrees around the z-axis.
- **Input****: "Move X1 to the right of X2."
****Output****:
``{'X1': 'X1.TRS_matrix @ translation_matrix(X2.Box[1][0] - X1.Box[0][0], 0, 0)}``
****Explanation****: The translation matrix is applied to the object X1 to move it to the right of object X2.
- **Input****: "Move X1 on top of X2."
****Output****:
``{'X1': 'X1.TRS_matrix @ translation_matrix((X2.Box[1][0] - X1.Box[0][0])/2, X2.Box[1][1] - X1.Box[0][1], (X2.Box[1][2] - X1.Box[0][2])/2)}``
****Explanation****: The translation matrix is applied to the object X1 to move it on top of object X2.
- **Input****: "Rotate X1 by 90 degrees around the x-axis and move it by 2 to the right."
****Output****:
``{'X1': 'X1.TRS_matrix @ translation_matrix(2, 0, 0) @ rotation_matrix(90, 0, 0)}``
****Explanation****: The translation matrix is applied to the object X1 to move it 2 units to the right, followed by a rotation of 90 degrees around the x-axis.

Additional Guidance for LLM:

- **ADHERE** strictly to the defined algebraic operations.
- **DO NOT** introduce any variables or constants not explicitly mentioned in the input.
- **DOCUMENT** each step: For every action you perform, you **MUST** provide a clear and numbered list of operations used during your reasoning.
- **REVISE** any transformation that does not comply with these principles.
- It is ****IMPORTANT**** to take into consideration all axis when performing relative transformations. Focus on the X ****AND**** Z axis when moving objects around the room. Make changes in the Y axis when a vertical movement is required. So, for example, when moving an object next to another, you should move it in both the X and Z axis, and when moving an object on top of another, you should move it in the X and Z axis, and also in the Y axis.
- When no axis is defined for rotations, the default axis is the Y-axis.
- When no unit is specified for the translation, the default unit is 1 and for the rotation, the default unit is 90 degrees.
- **MOVE ONLY** the objects that are mentioned in the query. Do not move any other objects in the scene.

Figure 6: Euclidean Prompt template for the Scene Editing Agent.

```

### Objective:
You MUST calculate the appropriate transformation for objects in a 3D space.
### Coordinate System:
- **X-axis (`e1`)**: Translates the object LEFT (-) or RIGHT (+).
- **Y-axis (`e2`)**: Translates the object BOTTOM (-) or TOP (+) height wise.
- **Z-axis (`e3`)**: Translates the object back (-) or forward (+).

You receive from the user the query to move objects in the 3D space. You must reason about the query in Euclidean Geometry and provide the transformation for each object in the scene.

You answer by only generating JSON files that contain the following information:

For each object you need to store:
- object_name: name of the object
- P_X: position of the object on X axis
- P_Y: position of the object on Y axis
- P_Z: position of the object on Z axis
- R_X: rotation of the object on X axis
- R_Y: rotation of the object on Y axis
- R_Z: rotation of the object on Z axis
- Length: dimension in cm of the object on X axis
- Width: dimension in cm of the object on Y axis
- Height: dimension in cm of the object on Z axis

Keep in mind, objects should be disposed in the area to create the most meaningful layout possible, and they shouldn't overlap.
Also keep in mind that the objects should be disposed all over the area in respect to the origin point of the area, and you can use negative values as well to display items correctly, since origin of the area is always at the center of the area.

### Example Inputs, Results in JSON format

The current scene is:
[
  {
    "object_name": "Parts_Pallet_1",
    "P_X": -150,
    "P_Y": 0.0,
    "P_Z": 250,
    "R_X": 0.0,
    "R_Y": 0.0,
    "R_Z": 0.0,
    "Length": 100,
    "Width": 100,
    "Height": 10,
  },
  {
    "object_name": "Boxes_Pallet_2",
    "P_X": -150,
    "P_Y": 0.0,
    "P_Z": 150,
    "R_X": 0.0,
    "R_Y": 0.0,
    "R_Z": 0.0,
    "Length": 100,
    "Width": 100,
    "Height": 10,
  }
]
1. **Input**: "Move the Parts_Pallet_1 to the right by 50 units."
**Output**:
[
  {
    "object_name": "Parts_Pallet_1",
    "P_X": -100,
    "P_Y": 0.0,
    "P_Z": 250,
    "R_X": 0.0,
    "R_Y": 0.0,
    "R_Z": 0.0,
    "Length": 100,
    "Width": 100,
    "Height": 10,
  }
]

```

Figure 7: Omniverse Prompt template for the Scene Editing Agent Part 1.


```

2. **Input**: "Rotate the Parts_Pallet_1 by 90 degrees around the z-axis."
**Output**:
[
  {
    "object_name": "Parts_Pallet_1",
    "P_X": -150,
    "P_Y": 0.0,
    "P_Z": 250,
    "R_X": 0.0,
    "R_Y": 0.0,
    "R_Z": 90.0,
    "Length": 100,
    "Width": 100,
    "Height": 10,
  }
]
3. **Input**: "Translate the Parts_Pallet_1 by 100 units to the right rotate it by 90 degrees around the z-axis."
**Output**:
[
  {
    "object_name": "Parts_Pallet_1",
    "P_X": -50,
    "P_Y": 0.0,
    "P_Z": 250,
    "R_X": 0.0,
    "R_Y": 0.0,
    "R_Z": 90.0,
    "Length": 100,
    "Width": 100,
    "Height": 10,
  }
]
4. **Input**: "Move the Parts_Pallet_1 on top of the Boxes_Pallet_2."
**Output**:
[
  {
    "object_name": "Parts_Pallet_1",
    "P_X": -150,
    "P_Y": 10.0,
    "P_Z": 150,
    "R_X": 0.0,
    "R_Y": 0.0,
    "R_Z": 0.0,
    "Length": 100,
    "Width": 100,
    "Height": 10,
  }
]
5. **Input**: "Move the Parts_Pallet_1 next to the Boxes_Pallet_2."
**Output**:
[
  {
    "object_name": "Parts_Pallet_1",
    "P_X": -250,
    "P_Y": 0.0,
    "P_Z": 150,
    "R_X": 0.0,
    "R_Y": 0.0,
    "R_Z": 0.0,
    "Length": 100,
    "Width": 100,
    "Height": 10,
  }
]
### Output Format:
The output MUST be formatted as a list of JSON objects, each containing the transformation for each object in the scene.

### Additional Guidance for LLM:
- ADHERE strictly to the defined algebraic operations.
- DOCUMENT Each Step: For every action you perform, you MUST provide a clear and numbered list of operations used during your reasoning.
- REVISE any transformation that does not comply with these principles.
- It's **IMPORTANT** to take into consideration all axis when performing relative transformations. Focus on the X **AND** Z axis when moving objects around the room. Make changes in the Y axis when a vertical movement is required.
So, for example, when moving an object next to another, you should move it in both the X and Z axis, and when moving an object on top of another, you should move it in the X and Z axis, and also in the Y axis.
- When no axis is defined for rotations, the default axis is the Y-axis.
- When no unit is specified for the translation, the default unit is 1 and for the rotation, the default unit is 90 degrees.
- MOVE ONLY the objects that are mentioned in the query. Do not move any other objects in the scene.

```

Figure 8: Omniverse Prompt template for the Scene Editing Agent Part 2.